to the Environmental Protection Agency on contract 68-02-2957, Environmental Protection Agency, Research Triangle Park, N.C., June 1981).

15. The plots may be found in (14). Some curvature in the lines is expected during the early portion of the reaction as NO is converted to NO_2, with little net loss of NO_x. Since our measurements were initiated after this conversion was largely complete, the potential curvature was not observed on most days.
16. The intercept is forced to zero by our definition that $[NO_x]_e = [NO_x]$ measured at time $t = 0$.
17. $$F_n = \frac{HNO_3 + PAN + NO_3^-}{NO + NO_2 + HNO_3 + PAN + NO_3^-}$$
18. For these flights, the total NO_3^- concentration in the plume ranged from 0.005 to 0.015 part per billion, with the higher values occurring at the longer irradiation times. The ratio of gaseous NO_3^- to total NO_3^- was greater than 0.95.
19. Such a parameterization for SO_2 conversion in power plant plumes has been reported by N. V. Gillani and W. E. Wilson, Jr., *Atmos. Environ.*, in press.
20. The results of further studies of the NO_x conversion rate, the reaction product distribution, and the influence of NO_x reactions on precipitation acidity will be reported elsewhere (C. Spicer, in preparation).

21. I am indebted to G. Sverdrup, G. Ward, J. Koetz, and W. Keigley for their assistance in field operations and data reduction and to R. Hannigan for aircraft operation. This project was sponsored by the Environmental Sciences Research Laboratory of the Environmental Protection Agency under contract 68-02-2957.

27 August 1981; revised 26 October 1981

Observations of a Comet on Collision Course with the Sun

Abstract. *A brilliant new comet (1979 XI: Howard-Koomen-Michels) was discovered in data from the Naval Research Laboratory's orbiting SOLWIND coronagraph. An extensive sequence of pictures, telemetered from the P78-1 satellite, shows the coma, accompanied by a bright and well-developed tail, passing through the coronagraph's field of view at a few million kilometers from the sun. Preliminary orbital calculations based on the observed motion of the comet's head and morphology of the tail indicate that this previously unreported object is a sungrazing comet and may be one of the group of Kreutz sungrazers. It appears from the data that the perihelion distance was less than 1 solar radius, so that the cometary nucleus encountered dense regions of the sun's atmosphere, was completely vaporized, and did not reappear after the time of closest approach to the sun. After this time, however, cometary debris, scattered into the ambient solar wind, caused a brightening of the corona over one solar hemisphere and to heliocentric distances of 5 to 10 solar radii.*

Comets are commonly classified, according to the period of their orbital revolution about the sun, into two groups. Short-period comets, distinguished by orbits of moderate eccentricity and small inclination to the ecliptic plane, have periods ranging from a few to about 200 years. Further, their orbits are usually direct (prograde); that is, their orbital angular velocities are directed in the same sense as the angular velocities of the planets. Long-period comets, with periods ranging up to millions of years, have trajectories oriented arbitrarily with respect to the ecliptic and with equal probability of being direct or retrograde. Their orbits are characterized by large eccentricity ($\epsilon \approx 1$) and indeed are often more conveniently described as parabolas than as ellipses. A remarkable subset of the long-period comets is the group of sungrazers, associated with the name of the 19th-century astronomer H. Kreutz, who analyzed the apparition in 1882 of a spectacular member of this group and reviewed the data on a number of other suspected members (1–3). This cometary group, which has been studied in recent times by Marsden (4), is marked by perihelion distances of 1 to 2 solar radii (1 $R_\odot$ = 696,000 km), and probably owes its origin to fragmentation of some earlier protocomet, whose nucleus may have fractured under the stresses of a near encounter with the sun. A prominent recent member of the group was the well-observed comet Ikeya-Seki (1965 VIII).

It is a frustrating characteristic of the Kreutz sungrazers that their common orbital path is oriented with respect to the solar system in such a way that they are difficult to observe from the earth, particularly if perihelion passage occurs during the months from May to August. At that time the comet, viewed from the earth, appears to approach the sun from behind at small angular separation and to recede in nearly the same direction (4). Thus, only members bright enough to be observed in twilit skies are seen. Furthermore, in several instances a comet was discovered only because a total solar eclipse occurred at a time nearly coincident with the comet's perihelion passage. The question has been raised, therefore, whether the total number of comets in sungrazing orbits far exceeds the number observed.

Background. We report here the discovery of a new comet (5) under circumstances closely akin to a solar eclipse, namely in data collected by the SOLWIND orbiting coronagraph, designed and built by the Naval Research Laboratory and operating aboard the U.S. Air Force Space Test Program's P78-1 satellite.

The SOLWIND coronagraph (6) is a small video telescope designed to monitor activity in the sun's white light corona in the annular region between 2.5 and 10 $R_\odot$. To do this it employs an external occulting disk held by a post 0.76 m in front of the objective lens of a Lyot coronagraph, after the technique originated by Koomen *et al.* (7, 8). The occulter artificially eclipses the sun, preventing the blinding direct light of the sun's photosphere from reaching the focal plane, or even the objective lens. This permits recording of coronal forms with typically about 10^{-9} times the photospheric brightness. The occulter further provides a radially varying vignetting function with transmission gradient adequate to allow single-exposure imaging of the corona even though the coronal brightness varies by an order of magnitude in the range 2.5 to 10 $R_\odot$. The images are recorded by a digitally scanned secondary electron conduction (SEC) vidicon during a 2.5-second exposure, then read out into the satellite telemetry system for storage in onboard tape recorders and subsequent transmission during passage over a ground station. The satellite is in a 97-minute polar orbit, synchronized into the noon-midnight plane. In normal operation, SOLWIND records a full-frame coronal image every 10 minutes during the sunlit portion of each orbital revolution, then turns off automatically during satellite nighttime, resuming operation at the next orbital dawn. Data gaps of several hours occur when duty cycling with other instruments is necessary.

Observations. The observations were made on 30 and 31 August 1979, but they have only recently become available for analysis owing to delays in release of the data tapes to experimenters. Three images of the solar corona as it appeared at that time (Fig. 1) illustrate the salient characteristics of the data. The coronal image is recorded as a matrix of 256 by 256 picture elements (pixels), each digitized to 8 bits. Pixels are spaced on 1.25-arc-minute centers. Figure 1a shows the typical appearance of the corona at this solar maximum period. Streamers are seen in every quadrant, even near the poles. The most striking feature of Fig. 1b is that the comet's image has completely saturated the display photograph (although the vidicon was not saturated). The comet's head, first observed at 1856 UT near 6 $R_\odot$ elongation from the sun, is brighter than any coronal form we have seen in data examined thus far, after more than 2½ years of operation. Pre-

0036-8075/82/0226-1097$01.00/0

liminary photometry indicates that it is comparable in brightness to Venus (magnitude ≈ −3.5), which is also in the coronagraph's field of view, having just passed superior conjunction. In the following paragraphs we describe our pre- and postperihelion observations as fully as possible, present a tentative, qualitative model that is consistent with the observations, and give the orbital parameters derived from this model.

Description of the data. Approach of the comet to perihelion is shown in Fig. 2a. The velocity, projected onto the plane of the sky, is 284 ± 12 km/sec. No acceleration is noted, within the limits of our accuracy; the path of the head does not deviate significantly from a straight line, nor does the projection of this line pass through the center of the solar disk. The tail is much more sharply defined along its southern edge (see Fig. 1 for orientation) than on the northern edge. These observational facts place constraints on the orbit calculation, forcing, for example, the conclusion that the observer is near, but not in, the orbital plane.

Figure 2b is a sampling of data during the postperihelion period. This phase is less simple to interpret, and detailed studies will be required before a complete explanation can be presented. The principal observations drawn from the data are as follows. (i) Tail material, strewn along the path of approach, persists for many hours after passage of the nucleus, growing even brighter in the period after perihelion than it was before occultation of the nucleus at 2115 UT. (We have no observations between 2115

Table 1. Range of parameters calculated for retrograde orbits in a sun-spacecraft coordinate system. The corresponding direct (prograde) solutions can be obtained by replacing α and β by $-\alpha$ and $-\beta$, respectively.

q ($R_\odot$)	T (UT)*	α (deg)	β (deg)	γ (deg)
0.12	2219 (2204)	22	5	41.9
0.25	2228 (2211)	17	0	42.5
0.50	2239 (2220)	12	−10	42.5
0.75	2245 (2229)	10	−20	42.4
1.00	2258	8	−25	41.8
1.50	2307	8	−40	42.7
2.00	2320	8	−50	43.4

*For solutions with $q < 1.0\ R_\odot$ the "impact" time is given in parentheses.

and 2344 UT.) (ii) This material diffuses and fades very slowly. The southern edge of the tail remains more sharply defined than the northern edge, which grows increasingly diffuse. Net mass motion is toward the north but the displacement, as projected on the plane of the sky, is very slow. (iii) While the tail material is diffusing away, another major diffuse brightening occurs. This brightening is extremely broad in angular subtense, filling almost an entire hemisphere and extending from the streak of tail material in the southwest 180° around to the northeast. The brightening appears to be somewhat concentrated in a narrower cone, of about 60° subtense, centered on the north. However, subtle changes occurring in the background corona at this time are superimposed on the cometary data (*9*). (iv) At no time do we observe anything interpretable as a cometary head from 2344 UT on 30 August through the first few days of September. (v) By 2036 UT on 31 August the excess material in the outer corona, in the hemisphere described above, has faded but not entirely dissipated. Its relative brightness distribution as a function of solar position angle has changed very little since 1109 UT on 31 August; it is much fainter and more diffuse, but still well above background noise levels. (vi) The diffuse brightenings described above, which we attribute to cometary debris, consist of light that is either unpolarized or only very slightly polarized (< 10 percent) (*10*).

Orbital calculations. Figure 3 shows a simple model that appears to be consistent with all available evidence. It also indicates the times at which images were recorded. We begin with a description of the orbit calculations.

The eight preoccultation images obtained during 1856 to 2115 UT on 30 August 1979 were used to estimate the comet's orbit. The apparent position of the comet's head was measured at each of these eight times. We then deduced the characteristics of assumed parabolic orbits whose projections onto the plane of the sky fit these measurements in both position and time within the measurement accuracy. In our sun-centered, plane-of-the-sky (r, θ) coordinate system, this accuracy was ± 0.1 $R_\odot$ in heliocentric distance, r, and ± 0.25° in position angle, θ, as determined by comparing observed positions of Venus and Regulus (α-Leonis) with their tabulated positions in the 1979 ephemeris (*11*).

The fitting procedure was accomplished by treating as a free parameter the heliocentric distance at perihelion, q,

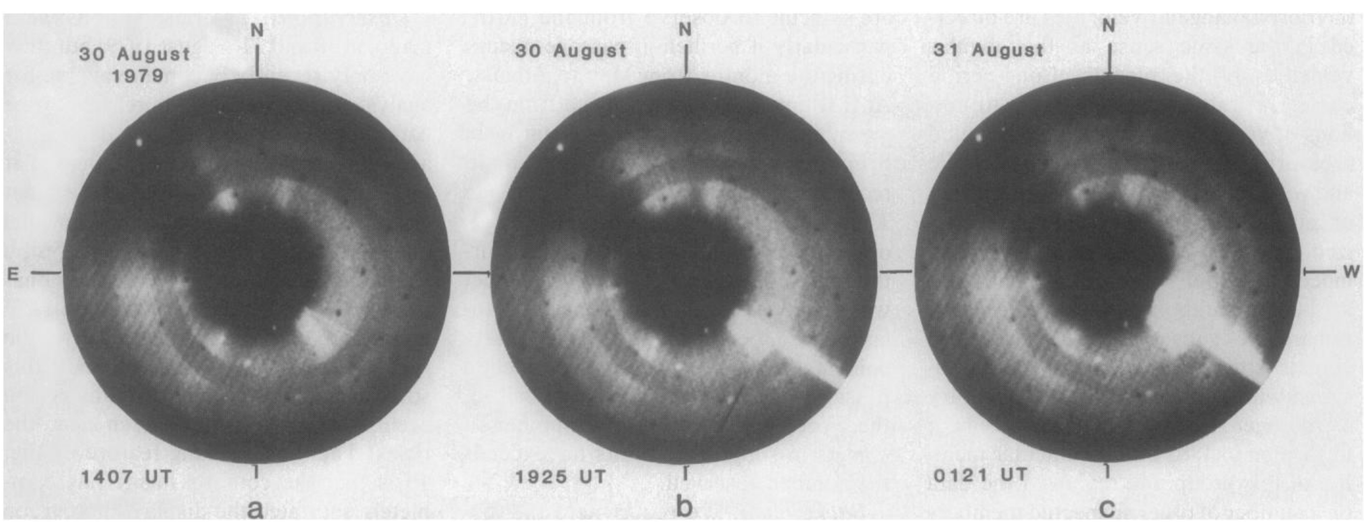

Fig. 1. The sun's outer corona as recorded by the SOLWIND coronagraph on 30 August 1979 at 1407 UT (a) and, after appearance of the comet, at 1925 UT (b). The central black area in each frame is the (deliberately out of focus) shadow of the occulting mechanism. The radius of this shadow is approximately 2.5 $R_\odot$. The instrumental field extends to 10 $R_\odot$ but has been cropped in these photos to about 8 $R_\odot$. The dark, nearly concentric rings are polarization analyzers [see text and (*7*)]. The shadowed region extending toward the upper left from the occulter shadow is caused by the occulter support pylon; the bright object just above it is Venus, which passed superior conjunction on 25 August. (c) Persistence and enhancement of glow caused by scattering from the tail debris are seen along the path of approach nearly 3 hours after dissolution of the cometary nucleus in the solar atmosphere.

which uniquely determines the form of the parabola in space, then adjusting the view angles and the time of perihelion passage, T, in an attempt to match to the observations the projected position as a function of time. It should be noted that the comet's head was observed for only 139 minutes, at a portion of the orbit very close to perihelion, and with resolution limited to 1.25 arc minutes. For this preliminary calculation, changes in aspect owing to the earth's orbital motion during the brief period of observation were neglected.

The resulting orbits fall into two classes, direct and retrograde. For each class it was possible to construct a range of solutions characterized by $0.12\ R_{\odot} \leq q \leq 2.0\ R_{\odot}$. For values of q outside this range, no combination of orientation angles or timing could match the observations within the measurement accuracy. Results of the calculations are presented with reference to two coordinate systems, one with the standard orbital elements, referenced to the ecliptic plane, used by astronomers for analysis of solar system kinematics. The other, more convenient for analysis of our satellite observations, involves an Euler angle transformation between a rectangular coordinate system aligned with the comet's orbit and one aligned with the satellite-to-sun line of sight. The transformation angles for the latter system are given in Table 1 and are included to provide a more intuitive picture of the observed event. In practice, the calculation was carried out in this system to determine α, β, γ, and T for selected values of q. Later the results were transformed to determine orbital elements in the standard format (Table 2). To a good approximation, α measures elevation of the line of sight with respect to the orbital plane, β is the angle by which the line of sight is skewed away from a broadside view (normal to the parabolic axis), and γ is a roll angle about the line of sight, giving the position angle of the parabolic axis, projected on the plane of

Table 2. Range of orbital elements calculated for retrograde orbits in a standard sun-centered, ecliptic coordinate system (equinox 1979.7). The corresponding direct (prograde) solutions can be obtained by replacing Ω, i, and ω by $\Omega - 180°$, $180° - i$, and $180° - \omega$, respectively.

q ($R_{\odot}$)	T (UT)*	Ω (deg)	i (deg)	ω (deg)	B (deg)	L (deg)
			Comet 1979 XI			
0.12	2219 (2204)	9.4	131.0	115.8	42.8	243.0
0.25	2228 (2211)	3.7	133.8	107.1	43.6	249.7
0.50	2239 (2220)	357.3	137.2	92.8	42.7	263.5
0.75	2245 (2229)	354.2	139.0	80.7	40.3	276.4
1.00	2258	351.1	139.9	73.5	38.1	282.3
1.50	2307	349.5	141.0	57.3	32.0	299.0
2.00	2320	348.0	141.4	46.2	26.8	308.8
			Comet 1965 VIII			
1.67	(21.18 October)	346.25	141.85	69.03	35.21	282.24

*For solutions with $q < 1.0\ R_{\odot}$ the "impact" time is given in parentheses.

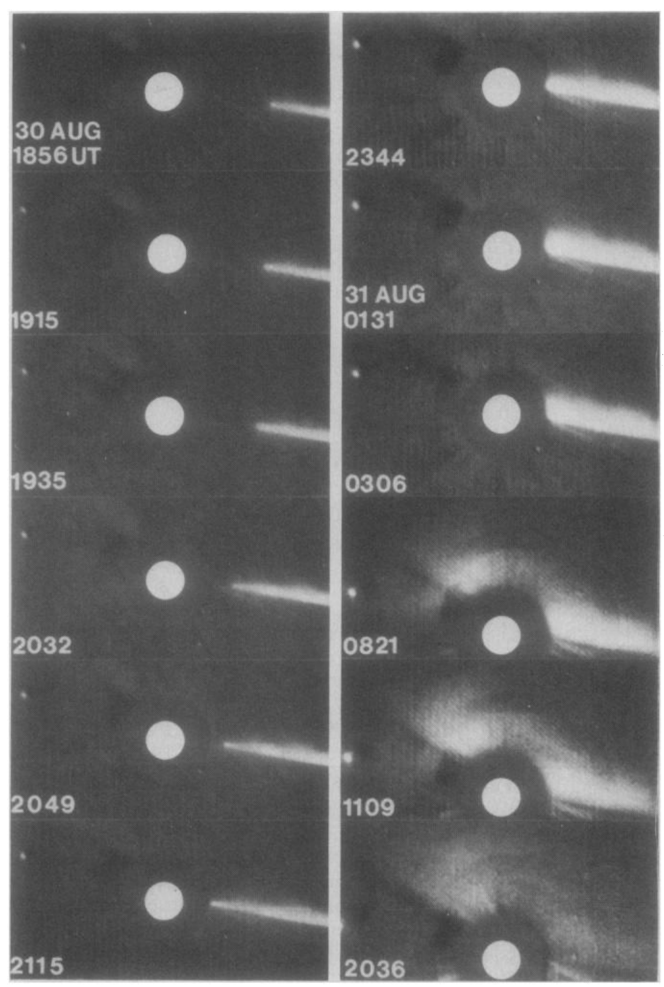

Fig. 2. Comet Howard-Koomen-Michels: difference images showing changes in the scene after about 1407 UT. Each frame consists of an image recorded at the given time, from which has been subtracted a pre-event image recorded at approximately 1407 UT on 30 August (Fig. 1a). A white disk has been placed at the center of the occulter shadow in each frame to show the location and scale size of the sun. The bright object to the left is Venus. (a) Preperihelion sequence. The coma approaches the sun with a velocity, projected on the plane of the sky, of 284 km/sec. The time of closest approach to sun center, perihelion, is estimated to have occurred between 2219 and 2258 UT, but somewhat before this the nucleus disintegrated on entering the solar atmosphere. (b) Postperihelion sequence. As the nucleus closes rapidly on the sun, evolution of gas and dust into the tail accelerates greatly. The first three frames (2344 UT on 30 August to 0306 UT on 31 August) show continued streaming of this material, driven radially outward by solar radiation pressure in the plane of the comet's orbit. Thus the tail appears brighter during this period than it did at 2115 UT on 30 August, when the head had just reached the occulter shadow, at 2.5 $R_{\odot}$. The effect is exaggerated here because the photographic contrast in (b) is enhanced relative to (a). After 0821 UT on 31 August, material is seen streaming outward in all directions, filling an entire hemisphere and presumably emanating radially from the site of final disintegration. This enhanced brightening persists until after 2036 UT, although in the later frames (0821 to 2036 UT) evolutionary changes in the background corona, superimposed on the cometary glow, are becoming evident.

the sky and measured southward from the solar west vector (12). Positive values of α correspond to view angles placing the observer below the orbital plane, and positive values of β correspond to views directed from the tail toward the nose of the parabola.

Tables 1 and 2 give the orbits calculated for a selection of q values spanning the range compatible with our measurements. The q's were chosen arbitrarily within the allowable range; they have not been subjected to any statistical criteria for best fit and may be considered about equally probable for present purposes. Note that solutions with larger perihelion distances have correspondingly smaller elevation angles, α; this is because larger parabolas must be viewed more nearly on edge in order to match the nearly linear path seen in our data. Also, larger values of q demand more negative values of β, because large parabolas must be observed at angles skewed farther from the broadside view (in the direction of nose to tail for retrograde orbits) to match the observed progression in time along the orbital path. The solutions for direct and retrograde orbits are symmetric in the sense that if (q_0, α_0, β_0, γ_0) is a solution for a direct orbit, then (q_0, $-\alpha_0$, $-\beta_0$, γ_0) is the corresponding retrograde solution. This degeneracy results from our neglect of the earth's orbital motion. Another refinement neglected in constructing Table 2 is the correction for precession of the equinoxes between the standard 1950.0 reference position and the 1979.66 date of our observations.

Interpretation. For comparison with the orbits of the sungrazers tabulated by Marsden (4), we have listed in Table 2 the ecliptic latitude, B, and longitude, L, of perihelion and have given Marsden's values for comet Ikeya-Seki, a representative member of the group. The remarkable agreement of the orientation angles strongly suggests that the newly discovered comet was a member of the group, which, in turn, argues in favor of adopting for the new comet the retrograde direction of motion characteristic of the Kreutz group.

Another factor tending to make retrograde orbits somewhat more probable than their direct counterparts is the circumstance that no sightings of this comet were reported despite its great brilliance. This may, of course, be fortuitous, or the object may have brightened suddenly only when it came very close to the sun. However, the retrograde orbits offer a simpler explanation in that they place the comet very close (in angle) to the sun for many days prior to perihelion (13), lessening the likelihood of detection from the ground. However, it is also true that the comet's position in the sky would make it visible only during morning twilight. Further, the orientation of the comet's tail is such that the best hope for detection would be from a location about 15° south of the equator, where the tail would stand approximately perpendicular to the horizon, but where observers are less numerous than at more northerly latitudes.

The range of permissible orbits is further reduced by consideration of the observations after 2344 UT on 30 August (see Fig. 3). (i) Orbits having $q > 1.75$ $R_\odot$ demand that the coma reappear on the far side of the occulting disk shadow, in the northeast, opposite the point of entry, starting at about 0100 UT. This is not observed, even though images are available for 0121, 0131, 0148, 0158, 0257, 0306, and so on. Thus we are forced to conclude that $q \leq 1.75$ $R_\odot$. (ii) All orbits having $q > 1.0$ $R_\odot$ require later reappearances of the coma in the southwest, at somewhat smaller position angles (more southerly) than that of the

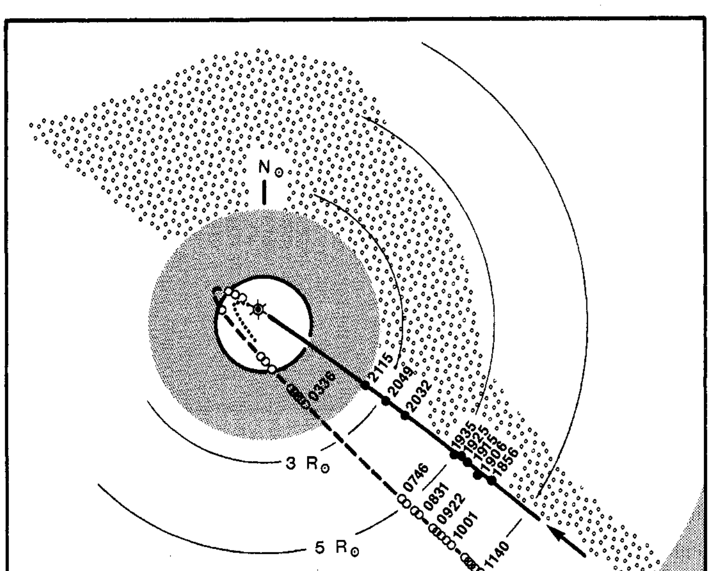

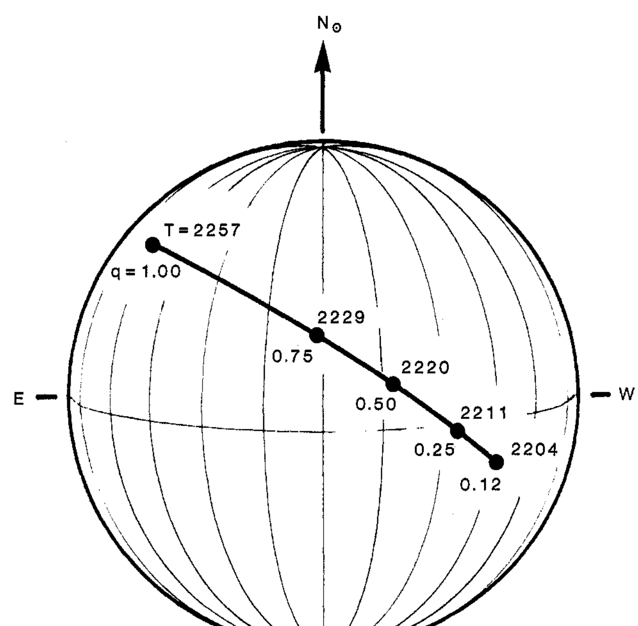

Fig. 3 (left). Calculated orbital paths for two different values of the perihelion distance, q. The first, shown by a solid line, is for $q = 0.75$ $R_\odot$. The closed circles superimposed on it show the position of the coma for each of the eight preoccultation observation times (1856 to 2115 UT). This calculated orbit predicts entry into the solar atmosphere at the location marked (*). Projection of the orbit beyond that point is shown by a dotted path interior to the sun. The broken line shows the result for a calculation based on $q = 1.1$ $R_\odot$, a reasonable near-miss value. The open circles superimposed on it indicate the times of coronagraph observations with corresponding calculated positions where the comet should have been observed (had it survived perihelion), but was not observed. The speckled area indicates the approximate extent of the diffuse glow that appeared later as disintegration products were driven outward by the solar radiation pressure (see Fig. 2). Fig. 4 (right). Solar coordinates and times of impact calculated for orbits listed in Tables 1 and 2. Numbers below the diagonal line give the assumed perihelion distance in units of $R_\odot$. Above the diagonal line are the corresponding times (UT) of intersection with the $r = 1.0$ $R_\odot$ surface for 30 August 1979. For retrograde orbits, the diagram represents the earth-facing solar disk.

approach path (234.5°). For example, for $q = 1.1\ R_\odot$, the distance of closest approach originally reported for comet Pereyra (1963 V), the orbit we calculate here would predict reappearance of the comet at 2.5 $R_\odot$ (emerging from the occulter shadow) at a position angle of 210° at 0430 UT on 31 August. The coma should then remain in the field of view until nearly 1800 UT on 31 August. It is not seen, although images are available throughout this period, starting at 0746 UT.

It can be argued that the comet did not collide with the sun ($q \leq 1.0\ R_\odot$), but simply lost all its volatile material through sublimation in a grazing encounter. While this is possible, it should be pointed out that the sublimation process exerts a profound cooling effect on cometary nuclei. Theoretical studies (*14*) indicate that even for sungrazing comets the thickness of the ice layer removed through sublimation in a single perihelion passage is not expected to exceed a few tens of meters, although fragmentation may be common in such events. Indeed comet Pereyra was discovered only after its grazing encounter with the sun (*15*); further, its perihelion distance was recalculated by Marsden (*4*) and by Sekanina (*16*) as only $q \leq 1.08\ R_\odot$, a scant 56,000 km above the photosphere.

The final point to be discussed in this connection is the relation of the proposed orbital model to the enhanced brightness distribution observed in the outer corona after the time of perihelion passage (Fig. 2b).

The first three frames in Fig. 2b are remarkable for the fact that the area strewn with cometary tail material contains far more excess brightness than was the case during the approach to perihelion (Fig. 2a). To understand how this is possible, we note that for particle diameters smaller than about 0.3 μm the outward radial force of the solar radiation field exceeds the gravitational attraction (*17*). Therefore small particles, once released, are quickly driven out of the comet's orbit and assume trajectories characterized by outward radial accelerations, but still in the comet's orbital plane. Thus some of the material visible in the early frames of Fig. 2b was released after passage of the nucleus behind the occulter at 2115 UT, as ablation proceeded at increasing rates with closer approach of the nucleus to the solar surface.

The situation is quite different for the last three frames of Fig. 2b, which show a widespread and diffuse brightening in areas north and west of the comet's approach track and tail. Particles responsible for this distribution appear to have experienced a history other than that of the tail particles, for (i) the observed radiance is considerably fainter and (ii) the scattering particles arrive at any given heliocentric distance hours after the tail particles, reaching a brightness maximum at about 0900 UT, when the tail brightness is fading.

It is possible that this broad fan of light emanated from particles in the comet's orbital plane. However, at the very great heliocentric distances required by the geometric projection, detection might be considered unlikely (*18*). We consider it more probable that these particles were driven out of the orbital plane, and that they were products of the final disintegration of the cometary nucleus in the solar atmosphere. That is, some portion of the nucleus was essentially stopped by atmospheric friction (*19*), and its decay products thermalized, that is, they acquired randomly directed velocities from the thermal motions of the surrounding medium. They were then blown outward by radiation pressure, with no "memory" of their previous orbital momenta. Particle trajectories in this case are determined by the radially outward solar radiation pressure and the random thermal velocities acquired in the dense regions of the solar atmosphere. Such a model produces a roughly conical distribution, somewhat resembling the ejection spray from a terrestrial explosion.

The fact that the resultant glow appears in the northern hemisphere of the corona, and not at all to the south of the comet's incoming path, indicates that the disintegration occurred in the northern hemisphere. Thus, assuming a retrograde orbit, we are viewing a broad cone, filled with disintegration products of the comet, having its apex on the near side of the solar disk and in the northern hemisphere; its axis, being radial, is tipped somewhat toward the observer (or away from the observer, with apex on the far side of the solar disk, for the case of a direct orbit).

No quantitative analysis of the brightness distribution within this diffusely glowing area has yet been undertaken. However, if it can be verified that the distribution is concentrated around a north-pointing vector, this would argue that the maximum stage of dissolution occurred close to the central meridian. It will be necessary to attempt removal of the underlying effects of coronal evolution before reaching a definite conclusion on this point.

In summary, our conclusions about the fate of the comet are based essentially on three factors: (i) calculated orbits are compatible with our preperihelion observations only for $0.12\ R_\odot \leq q \leq 2.0\ R_\odot$, (ii) postperihelion observations show that the comet never reappeared from behind the occulting disk after the time of perihelion passage, and (iii) a great amount of cometary debris seems to be scattered out of the comet's orbital plane, implying major departure from a gravitational orbit. Thus, while the details of its demise are not known with certainty at this point, it appears from the data that this comet did not survive its solar encounter of 30 August 1979.

In constructing the sketch of Fig. 3, we used as a working model the case $q = 0.75\ R_\odot$. This corresponds to a perihelion time of 2245 UT, but the computed orbital path intersects the photosphere ($r = 1.0\ R_\odot$) at 2229 UT. The coordinates of this entry point, projected on the solar disk as viewed from the earth, are 0.23 $R_\odot$ from disk center at a position angle 7.3° (measured eastward from solar north).

This point is shown in Fig. 4, along with the predicted impact times and coordinates for the other orbits listed in Tables 1 and 2. So far, no obvious correlation with surface phenomena has been discerned. This may not seem surprising. However, the possibility of observing some surface manifestation of a cometary impact on the sun is not negligible. The kinetic energy of a cometary nucleus, with an assumed radius of 1 km, density of 1 g/cm^3, and velocity of 284 km/sec, is some 1.7×10^{30} ergs, comparable with the energy release of a solar flare. At this stage one can only speculate on the volume through which this energy might have been distributed, but the volume associated with a chromospheric ribbon flare, corresponding to an atmospheric entry path length on the order of 10,000 km, does not seem unreasonable on geometric grounds.

Cometary versus coronal material. In the preceding discussion we assumed that most of the glow recorded by the coronagraph during the period described was produced by photospheric light scattered from released cometary dust or grains. This assumption is supported by the polarization information contained in the data.

In the original, unsubtracted images (Fig. 1), polarization analyzer segments of the focal plane are visible as dark rings, because the streamers and background K-corona are produced by photospheric light Thompson-scattered from free electrons in the fully ionized coronal plasma. This light is highly polarized, with the electric vector in a plane normal to the radius vector. Hence the rings, which are designed to pass only radially polarized light, appear dark. The contrast between this behavior and that of the comet is seen clearly in Fig. 1b, where the bright southwest streamer is almost completely cut off by the analyzer ring at 5 $R_{\odot}$, while the comet tail is nearly unaffected.

In some of the enhanced frames of Fig. 2, a very slight effect of the analyzer may be barely perceptible at the more diffuse (northerly) edge of the tail. This is expected because material separated from the cometary nucleus by solar heating undergoes selective acceleration (*17*), producing a distribution spectrum of particle sizes. As the released material is driven farther from the cometary orbit, the separation according to grain size becomes more pronounced. Large grains, 1 to 10 μm or more in diameter, remain for some time near the original orbit path. They produce, in the aggregate, an appearance similar to an aircraft's "contrail" in the upper atmosphere, although individual particles continue to orbit with velocities close to that of the comet's head. Smaller particles are driven away from the original parabola more rapidly than the large ones. In this cosmic winnowing process, when a substantial fraction of the grains in a certain area are much smaller than the wavelength of the incident photospheric light (<< 0.5 μm), the scattering process will best be described by Rayleigh theory (*20*) and polarization at right angles to the illuminating rays should be evident. No net polarization is expected for the larger particles.

Conclusion. We have reported the observation of a new comet, apparently the first to be discovered from a spacecraft and the first observed to collide with the sun. Preliminary analysis has provided a set of orbital elements of modest accuracy and suggests that the comet may be one of the Kreutz sungrazers. Disintegration products from the encounter caused a major change in the coronal brightness distribution, which persisted for more than one full day. Indications of the encounter on the solar surface have not yet been identified but are a distinct possibility. We invite other researchers to communicate to us any corroborative observations of either solar surface or coronal manifestations of this unusual observation.

D. J. MICHELS
N. R. SHEELEY, JR.
R. A. HOWARD
M. J. KOOMEN

E. O. Hulbert Center for Space Research, Naval Research Laboratory, Washington, D.C. 20375

References and Notes

1. H. Kreutz, *Publ. Sternw. Kiel No. 3* (1888).
2. ——, *ibid., No. 6* (1891).
3. ——, *Astron. Abhandl.* **1** (No. 1) (1901).
4. B. G. Marsden, *Astron. J.* **72**, 1170 (1967).
5. ——, *Int. Astron. Union Circ. No. 3640* (1981); *ibid., No. 3647* (1981).
6. N. R. Sheeley, Jr., D. J. Michels, R. A. Howard, M. J. Koomen, *Astrophys. J.* **237**, L99 (1980).
7. A complete description of a similar instrument, flown on OSO-7, has been given by M. J. Koomen, C. R. Detwiler, G. E. Brueckner, H. W. Cooper, and R. Tousey [*Appl. Opt.* **14**, 743 (1975)]. The SOLWIND coronagraph is optically almost identical to the OSO-7 instrument, but has greatly improved data rate and storage capabilities.
8. B. Lyot, *C. R. Acad. Sci.* **191**, 834 (1930).
9. For example, the streamer prominent in the north-northeast at 1407 UT on 30 August (Fig. 1) has faded markedly by 0121 UT on 31 August. This is reflected in the difference image shown in the 1109 UT frame of Fig. 2b as a darkened swath in the position formerly occupied by the streamer. Note that the frame marked 1109 UT in Fig. 2b is a difference image, consisting of data recorded at 1109 UT on 31 August minus an image recorded at 1417 UT on 30 August.
10. A complete description of the polarization analyzer system is given by Koomen *et al.* (*7*).
11. *American Ephemeris and Nautical Almanac—1979* (Government Printing Office, Washington, D.C., 1977), pp. 231 and 336.
12. The transformation is more precisely defined as follows. Suppose that the parabola lies in the xy plane and that the parabolic axis and the y axis coincide. Then consecutive rotations R_α (about y), R_β (about z'), and R_γ (about x'') lead to a rectangular coordinate system $x''y''z''$ in which the x'' axis is the line of sight and the z'' and y'' axes are the directions of solar north and west, respectively, projected onto the plane of the sky.
13. B. Marsden, private communication.
14. W. F. Huebner, *Z. Astrophys.* **65**, 185 (1967).
15. See section V of (*4*).
16. Z. Sekanina, *Int. Astron. Union Circ. No. 1993* (1967).
17. Because the radiative flux density and the gravitational force both vary as the inverse square of heliocentric distance, the ratio of the gravitational attraction to the repulsive radiation force is a constant, depending on the particle's size, density, and optical properties. Values typical for the interplanetary dust, which we here assume are applicable to the cometary dust, are given by S. F. Singer, in *Solar Physics*, J. M. Xanthakis, Ed. (Interscience, New York, 1967), p. 485.
18. From projection geometry alone we cannot distinguish whether the widely dispersed cometary material is in or out of the orbital plane, or both. If in the plane, a 6-$R_{\odot}$ projection in the plane of the sky represents cometary material between 16 and 43 $R_{\odot}$ distant from the sun, where it would presumably have a very low brightness, as both particle density and radiative flux density are expected to fall off as r^{-2}. Photometric and other studies may help to define the distribution.
19. In addition to heating, the atmospheric drag reduces an incoming body's velocity, dropping it to lower orbits, so that the atmospheric entry process is a self-accelerating one. For a homely comparison, densities in the solar chromosphere are on the order of 10^{-11} g/cm^3, comparable to regions in the earth's ionosphere, at 75 to 100 km, at which altitudes meteoroids are routinely observed by their glowing trails against the nighttime sky.
20. For example, see M. Born and E. Wolf, *Principles of Optics* (Pergamon, New York, 1959), chap. 13.
21. We wish to acknowledge a debt of gratitude to B. Marsden, F. Whipple, and E. Roemer for their insights and helpful discussions. In the experimental area, many persons have contributed to the successful development and long orbital lifetime of the SOLWIND coronagraph. We gratefully acknowledge the dedication with which D. Roberts, F. Harlow, R. Chaimson, R. Seal, W. Funk, D. Conroy, R. Perlut and R. Davies assisted in design, preparation, and test of the instrument. We are indebted to the Space Test Program, administered by the U.S. Air Force for the Department of Defense, for P78-1 spacecraft integration, launch, and operational support; to the Air Force Satellite Control Facility MCC-F team for patience and perseverance in the on-orbit operations that produced these observations; and to the NASA Office of Space Science for contribution of extensive hardware inventories that made possible development of the necessary solar pointing control. Finally, we thank R. Gilbert of the Ball Aerospace Division and his engineering team for outstanding performance in design and implementation of the spacecraft systems and interfaces.

21 October 1981

Development of a Monoclonal Antibody Against a Tumor-Associated Antigen

Abstract. *A monoclonal antibody-producing hybrid cell line was obtained by fusing mouse myeloma cells with spleen cells from a mouse immunized with C6 glioma cells. This antibody binds to a specific cell-surface antigen that is present on C6 rat glioma cells, transformed astrocytes and oligodendrocytes, and a human glioma cell line but is absent on a normal glial cell line, fibroblasts, and primary cultures of astrocytes and oligodendrocytes. The antigen also appears on tumor tissue of transformed oligodendrocytes but not on normal brain tissue.*

The nature of neoplastic transformation has been the object of numerous investigations in a variety of tissues (*1*), but the literature on the study of brain neoplasms is scant. The potential targets of neoplastic transformation in the brain are its three main cell types, the neurons and the principal glial cells, namely, the oligodendrocytes and the astrocytes. A major obstacle to the detailed study of tumor induction in brain is the overwhelming complexity of the intricate interactions among these various cell types that greatly hinders experimental design and data interpretation. This problem was overcome by the development in our laboratory of a novel technique [McCarthy and de Vellis (*2*)] to grow separate cultures of oligodendrocytes and astrocytes. Use of the homogeneous cell populations has greatly facilitated investigations into the changes that occur specifically during glial transformation. Recently, Bressler *et al.* (*3*) demonstrated that both astrocytes and oligodendrocytes can undergo spontaneous or ethylnitrosourea (ENU)-induced transformation. We now report the development of a monoclonal antibody that binds specifically to the surface of transformed glial